Supplementary Information For:

Bending Good Beats Breaking Bad: Phase Separation Patterns in Individual Cathode Particles upon Lithiation and Delithiation

David A. Santos,[1,2]† Justin L. Andrews,[1,2]† Yang Bai,[3]†, Peter Stein,[3] Yuting Luo,[1,2] Yuwei Zhang,[4] Matt Pharr,[4] Bai-Xiang Xu,[3]* Sarbajit Banerjee[1,2]*

[1]Department of Chemistry, Texas A&M University, College Station, TX, 77843-3255, USA.

[2]Department of Materials Science and Engineering, Texas A&M University, College Station, TX 77843-3255, USA.

[3]Institute of Materials Science, Mechanics of Functional Materials, Technische Universität Darmstadt, Otto-Berndt-Str. 3, 64287 Darmstadt, Germany.

[4]Department of Mechanical Engineering, Texas A&M University, College Station, Texas 77840, USA.

*Bai-Xiang Xu, Sarbajit Banerjee

Email: xu@mfm.tu-darmstadt.de, banerjee@chem.tamu.edu

†These authors contributed equally to this work

This supplemental file includes:

- **Supplemental Methods**
- **Fig. S1** Lithiation induced phase transformations in $Li_xV_2O_5$ and the corresponding galvanostatic charge/discharge curve.
- **Fig. S2** Powder X-ray diffraction and electron microscopy of as-synthesized V_2O_5 nanowires
- **Table S1.** Refined lattice parameters for the Rietveld refinement shown in Fig. S2.
- **Table S2.** Atom positions refined during the Rietveld refinement shown in Fig. S2.
- **Fig. S3** Comparison of spectra collected for stoichiometrically lithiated V_2O_5.
- **Fig. S4** Change in vanadium coordination environment across the ε↔δ phase transition.
- **Movie. S1**–**S6**. Phase-field modeling of phase separation patterns in the presence of distinct interfacial energetics
- **Supplemental References**

Supplemental Methods

Powder X-ray diffraction (XRD) and Rietveld refinement

Powder X-ray diffraction (XRD) patterns were collected in Bragg-Brentano geometry on a Bruker D8-focus diffractometer (Cu K-α, λ = 1.5418 Å; 40 kV voltage; 25 mA current). Rietveld refinement was performed using the GSAS II software suite.[1]

Synthesis of Stoichiometric $Li_xV_2O_5$ Phases for X-ray Absorption Standards

When *n*-butyllithium is used as a chemical lithiation reagent, the intercalation reaction is irreversible (resulting in the formation of octane – see Eq. (5). As shown in seminal experiments by Whittingham, samples lithiated by *n*-butyllithium model electrochemical conditions wherein kinetic conditions lead to some measure of inhomogeneity.[2,3] Alternatively, lithium iodide can be used to achieve phase purity, according to the following reaction:

$$V_2O_5(s) + xLiI(acetonitrile) \leftrightarrow Li_xV_2O_5(s) + \frac{x}{2}I_2(acetonitrile) \qquad \text{(S1)}$$

The product formed from this reaction is I_2, which acts as a mild oxidant and chemical deintercalation agent. As a result, the reaction is reversible.

As synthesized V_2O_5 nanowires (300 mg) were dispersed using stirring in dry acetonitrile under an inert Ar atmosphere. A 1.25 molar excess of the desired stoichiometric amount of LiI (anhydrous) was added to the acetonitrile/V_2O_5 mixture and was allowed to stir for one week to achieve phase purity. The 1.25 molar excess was employed to account for the reverse reaction (i.e., not all LiI reacts and a 1.25 molar excess accounts for this). The $Li_xV_2O_5$ powders were separated from the supernatant (which was a brown color owing to the formation of acetonitrile) by centrifugation and washed 3× with dry acetonitrile to remove I_2 and excess unreacted LiI. The powder products were allowed to dry under an inert atmosphere. The phase purity of these materials was determined by powder X-ray diffraction. These stoichiometric $Li_xV_2O_5$ "standards" were used to collect XAS spectra (Fig. S3 Supplementary Information) representative of key regions in the V_2O_5-LiV_2O_5 phase diagram.

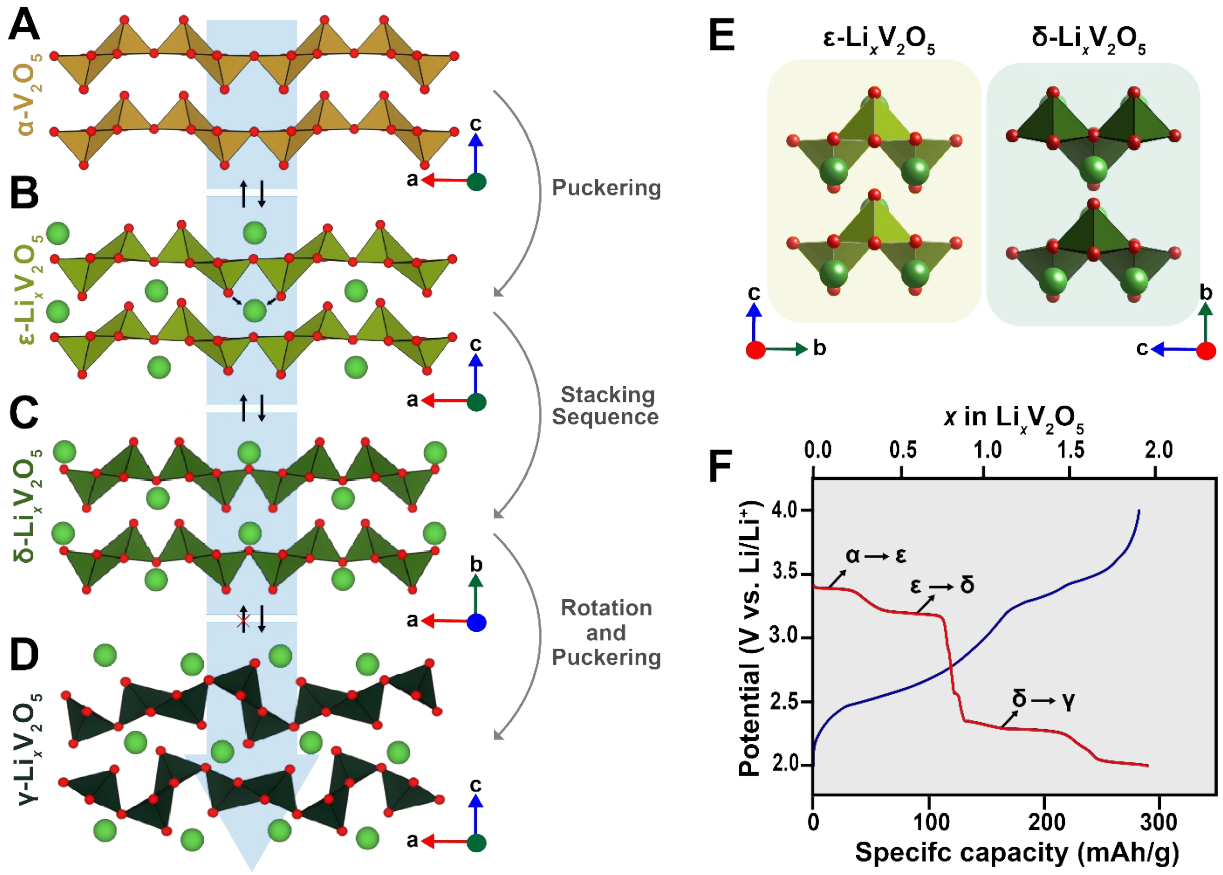

Fig. S1 Lithiation induced phase transformations in $Li_xV_2O_5$ and the corresponding galvanostatic charge/discharge curve. **(A–D)** Lithiation-induced crystal structure transformations of $Li_xV_2O_5$. For $x < 1$ in $Li_xV_2O_5$, the (A) α-, (B) ε-, and (C) δ-phases are stabilized within lithium concentration windows of ca. $0.0 < x < 0.1$, $0.3 < x < 0.7$, and $0.9 < x < 1.0$, respectively. These transformations are entirely reversible. Higher extents of lithiation ($x > 1$ in $Li_xV_2O_5$) bring about an irreversible transformation to the γ-$Li_xV_2O_5$ phase for $1 < x < 2$ (D). **(E)** The crystal structures of ε- and δ-phase of $Li_xV_2O_5$ are depicted as viewed down the crystallographic *a*-axis, illustrating the difference in V_2O_5 layer stacking between α/ε-$Li_xV_2O_5$ and δ-$Li_xV_2O_5$. Note that the α-, and ε- phases are in the same space group whereas the δ-phase is in the *Amam* space group and exhibits a doubling of the unit cell along the *b* axis to account for the break in symmetry resulting from the half-unit cell shift shown in (E). Critically, the half unit cell shift dramatically alters the coordination environment of the vanadium sites from a distorted quasi-octahedral environment to a predominantly square-pyramidal environment. This change in the coordination environment changes the crystal field splitting, which is reflected in

substantial changes of the O K-edge manifold in XANES spectra. **(F)** Galvanostatic discharge/charge profiles measured for V_2O_5 cycled at a C-rate of 0.05C in a coin cell configuration. Phase transitions are indicated above the plateau regions. Owing to the irreversibility of the δ↔γ transition, the charging curve is flattened as the γ-phase is delithiated from $x = 2$ to $x = 0$ without any significant rearrangement of the V-O structure.

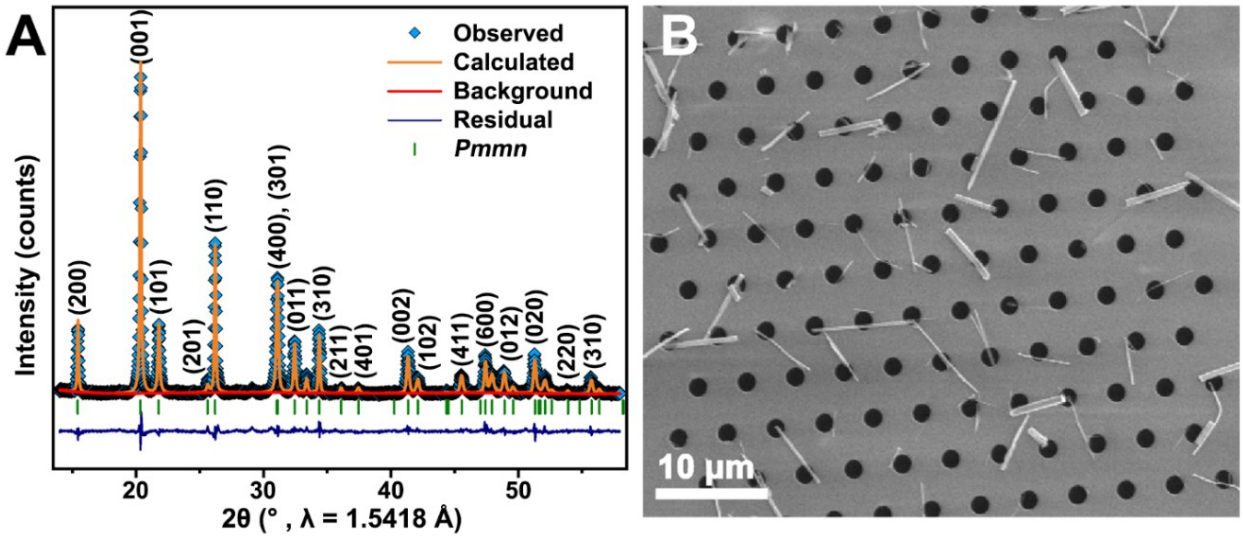

Fig. S2 Powder X-ray diffraction pattern and scanning electron microscopy image of V_2O_5 nanowires. **(A)** Powder X-ray diffraction (XRD) pattern of as-synthesized V_2O_5 nanowires. Rietveld refinement to the data was performed to confirm phase purity (see also Tables S1 and S2). A strong preferred orientation is evident in the pattern, stemming from the 1D nanowire morphology of the sample. Parameters extracted from Rietveld refinement of XRD patterns are provided in Tables S1 and S2. **(B)** Scanning electron microscopy image of V_2O_5 nanowires drop-cast onto an amorphous silicon nitride grid.

Table S1. Refined lattice parameters for the Rietveld refinement shown in Fig. S2. Refinement statistics are provided at the top of the table. Standard errors for refined parameters are provided in parentheses.

$X^2 = 2.877$, wRp = 7.67%, Rp = 5.89%	
Lattice Parameter	**Distance**
a (Å)	11.5004(3)
b (Å)	3.56112(7)
c (Å)	4.36758(8)
V (Å^3)	178.871(6)

Table S2. Atom positions refined during the Rietveld refinement shown in Fig. S2. The thermal parameters were held constant and not refined.

Atom	***x***	***y***	***z***
V	0.1005(2)	0.25	0.8956(5)

O1	0.1088(5)	0.25	0.5306(12)
O2	-0.0797(7)	0.25	0.0071(12)
O3	0.25	0.25	0.0071(18)

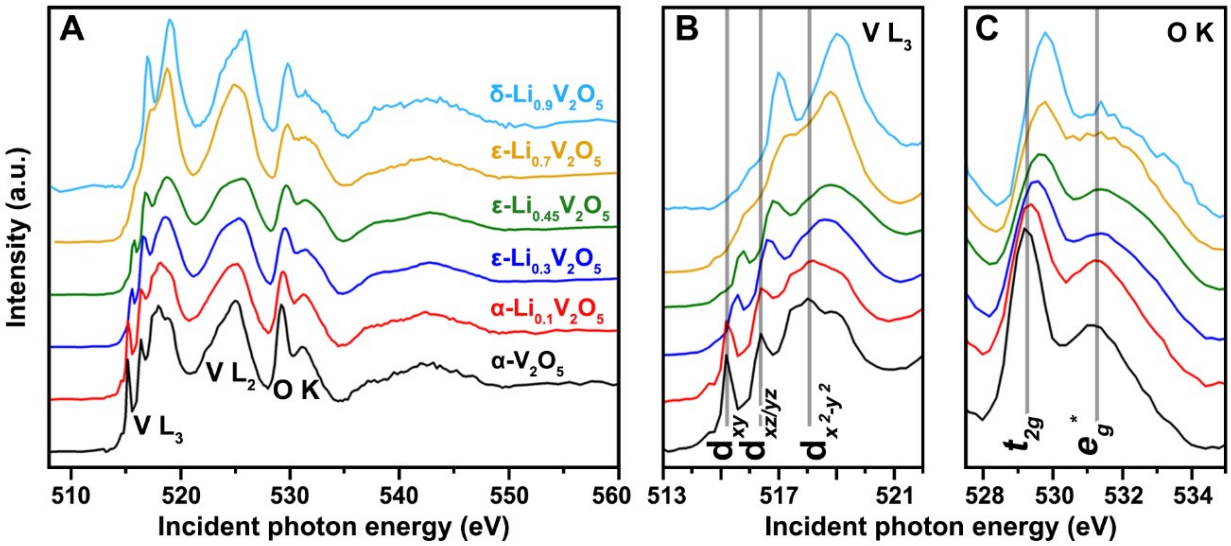

Fig. S3 X-ray absorption near-edge structure (XANES) spectra collected for stoichiometrically lithiated V_2O_5 with varying extents of lithiation. **(A)** Combined V L- and O K-edge spectra collected for stoichiometrically lithiated phases of V_2O_5. Expanded views of the XANES spectra are provided for **(B)** the V L_3-edge and **(C)** the O K-edge and are labeled with the final states of the transitions.

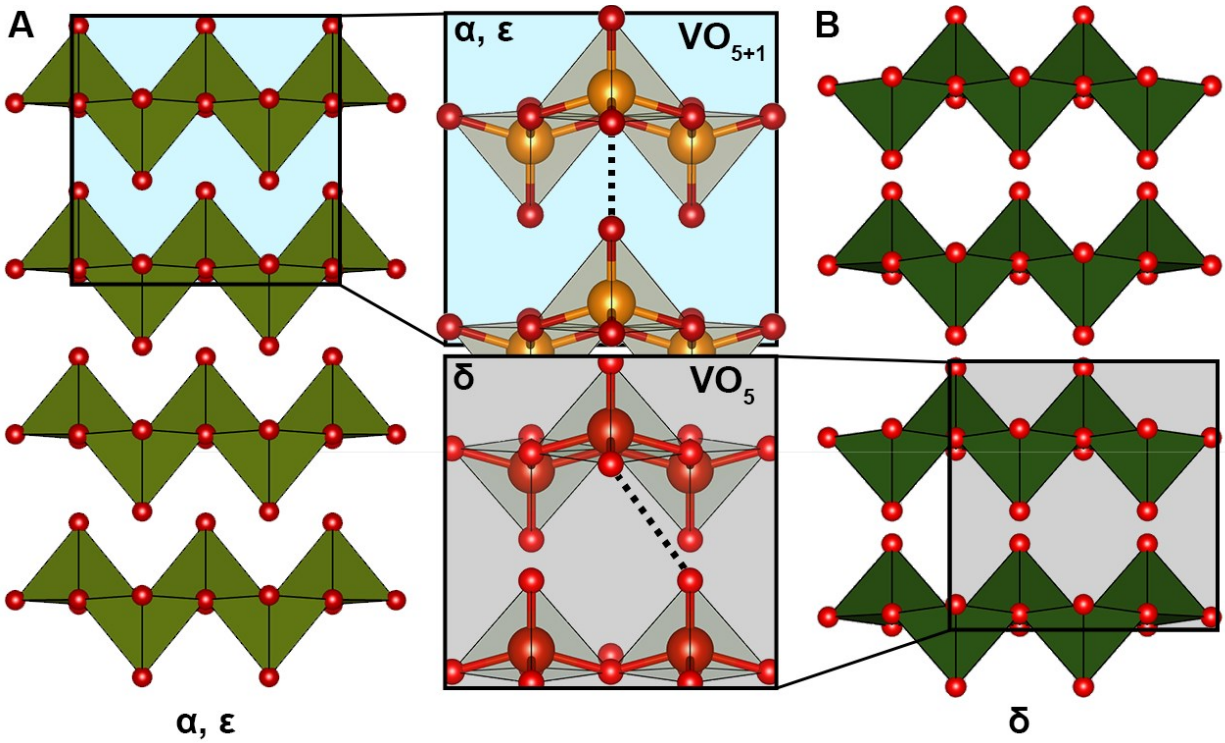

Fig. S4 Change in vanadium coordination environment across the ε↔δ phase transition. **(A)** illustrated the coordination enviorment of the α and ε phases wherin the layers pucker with increasing lithiation but the layer stacking is retained, and the vanadium coordination environment is also retained. **(B)** Highlgihts the difference in coordination enviorment for the δ phase; here the layer stacking is altered, and the vanadium coordination environment is changed dramatically. The structures shown in (A) and (B) were adapted from previously published diffraction data[4] in supplemental reference [4].

Movies S1–S6. Phase-field modeling of phase separation patterns in the presence of distinct interfacial energetics. Movies S1–S6 simulate the evolution of phase separation patterns during lithiation in the presence of distinct interfacial energetics quantified by the interface parameter κ with values of 1×10^{-11}, 2×10^{-11}, 5×10^{-11}, 1×10^{-10}, 5×10^{-10}, and 1×10^{-9}, respectively. Related to Fig. 4 C–H, main manuscript.

Supplemental References:

1 B. H. Toby and R. B. Von Dreele, *J. Appl. Crystallogr.*, 2013, **46**, 544–549.

2 L. R. De Jesus, G. A. Horrocks, Y. Liang, A. Parija, C. Jaye, L. Wangoh, J. Wang, D. A. Fischer, L. F. J. Piper, D. Prendergast and S. Banerjee, *Nat. Commun.*, 2016, **7**, 12022.

3 M. S. Whittingham and M. B. Dines, *J. Electrochem. Soc.*, 1977, **124**, 1387.

4 J. Galy, C. Satto, P. Sciau and P. Millet, *J. Solid State Chem.*, 1999, **146**, 129–136.